oxide film β increases linearly with time, implying a rate-determining step for film growth independent of transport in this layer. From a point of view of corrosion science, the evolution of film β is associated with the breakdown of passivity rendered to Pt by oxide film α, and can be thus described as "transpassive behavior of Pt in aqueous H_2SO_4."

REFERENCES

1. S. Gottesfeld, M. Yaniv, D. Laser, and S. Srinivasan, *J. Phys. (Paris), Colloq.,* **C5,** 145 (1977).
2. G. Tremiliosi-Filho, G. Jerkiewicz, and B. E. Conway, *Langmuir,* Submitted for publication.
3. S. Shibata and M. Sumino, *Electrochim. Acta.,* **17,** 2215 (1972).
4. S. Shibata, *ibid.,* **22,** 175 (1977).
5. S. Shibata, *J. Electroanal. Chem.,* **89,** 37 (1978).
6. H. Angerstein-Kozlowska, B. E. Conway, and W. B. A. Sharp, *ibid.,* **43,** 9 (1973).
7. Manual for the Automatic S-2000 Ellipsometer (Rudolph Research).
8. Handbook for Optical Constants of Solids, E. D. Palik, Editor, pp. 340-341, Academic Press (1985).
9. B. D. Cahen, J. Horkans, and E. Yeager, *Surf. Sci.,* **37,** 559 (1973).
10. S. Gottesfeld, in "Electroanalytical Chemistry," Vol. 15, J. Bard, Editor, Marcel Dekker (1989).
11. D. W. Marquardt, *J. Soc. Ind. Appl. Math.,* **11,** 431 (1963). See also K. Levenberg, *Q. Appl. Math.,* **2,** 164 (1944).
12. F. M. P. M. Habraken, O. L. J. Gijzeman, and G. A. Bootsma, *Surf. Sci.,* **96,** 482 (1980).
13. J. Rishpon and S. Gottesfeld, *This Journal,* **131,** 1960 (1984).
14. M. Pourbaix, "Atlas D'Equilibres Électrochimiques," pp . 379-383, Gauthier-Villars, Paris (1963).
15. C. T. Chen and B. D. Cahan, *This Journal,* **129,** 17 (1982).
16. W. Schmickler, in "Passivity of Metals and Semiconductors," M. Froment, Editor, p. 23, Elsevier (1983).
17. R. W. Collins and Y. T. Kim, *Anal. Chem.,* **62,** 887A (1990).

Electrochemical and Scanning Tunneling Microscopic Study of Dealloying of Cu₃Au

Thomas P. Moffat,* Fu-Ren F. Fan, and Allen J. Bard*

Department of Chemistry, The University of Texas at Austin, Austin, Texas 78712

ABSTRACT

Dealloying of Cu₃Au has been examined by *in situ* STM and several electrochemical methods. Three different regimes of behavior were noted. At low overpotentials, clustering of gold atoms occurs near sites of copper dissolution. This is essentially a two-dimensional process. The formation and smoothing of these clusters by capillary action, monitored in real time, demonstrated the highly mobile nature of the surface species. At higher potentials, the electrode is largely passivated by the enrichment of gold. However, there exist small localized regions of three-dimensional roughness which may be correlated to extended dealloying catalyzed by bulk solid-state defects. When the potential is increased above the critical potential (E_c), global surface roughening occurs. Correlating STM with chronoamperometric and chronopotentiometric results demonstrates that this transition occurs by nucleation and growth. Selective dissolution of copper depends on the exposure of fresh sites by the migration of passivating gold atoms. Adsorption can strongly influence this transport process, as manifest by changes in E_c. In comparison to sulfate media, chloride caused a decrease in E_c, while derivatization of Cu₃Au with an alkyl-thiol produced an increase in E_c. These shifts are consistent with the enhancement and inhibition of gold surface diffusion by the respective adsorbates.

Dealloying is a phenomenon of great importance in general corrosion (1, 2), stress corrosion cracking (2, 3), and catalysis (4). In the case of a binary alloy A-B, such as Cu-Au, dealloying entails the selective dissolution of the less-noble element A, in this case, copper. A schematic of a typical potentiostatic polarization curve is given in Fig. 1. The curve exhibits a domain of very low potential-independent current followed by a region of rapidly increasing current. The potential defining the transition between these regimes is known as the critical potential, E_c. E_c is a strong function of alloy composition (1, 2). At potentials below E_c, dissolution of the active species, A, leads to an enrichment of the noble species B, in this case, gold, which suppresses the further dissolution of A. It is unclear if this blocking layer is pure B, or a B-enriched alloy. The critical potential is associated with the breakdown of this passivating overlayer and the onset of massive dealloying. At potentials greater than E_c, gross surface roughening occurs and the near-surface of the alloy evolves into a fine, porous, noble-metal enriched network. This process has

been described as a cellular-phase transformation (4). It has been suggested that the critical potential, E_c, defines the transition from a stable planar surface to a highly ramified interface (2).

A variety of mechanisms have been proposed to explain the breakdown phenomenon that leads to massive dealloying. Modern discussions have largely concentrated on the relative importance of volume diffusion *vs.* surface transport processes (1). Pickering and Wagner (5) suggested that the rate of dealloying is controlled by solid-state diffusion of the less-noble metal via divacancies. Prior to this, Wagner (6) demonstrated that if volume diffusion controls the rate of dealloying, then geometrical instabilities will develop along the planar interface which will grow rapidly with time. This could account for the sponge-like morphology of the dealloyed layer. The critical potential was ascribed to a potential-dependent concentration of divacancies (2). The large increase in defect density would occur at high overpotentials where oxidation from highly coordinated surface sites becomes possible. This mechanism depends on the blocking layer being B-enriched as opposed to a pure B overlayer. An alternative dealloying mecha-

---

* Electrochemical Society Active Member.
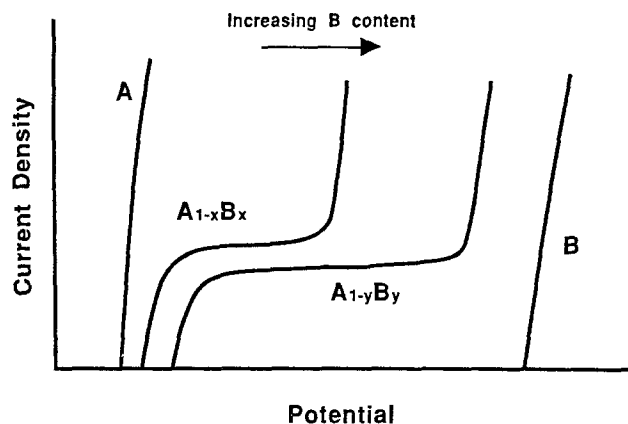
Fig. 1. Schematic of the polarization behavior of binary alloys.

nism based on surface diffusion was proposed by Gerischer *et al.* (7), where the surface mobility of the more noble element governs the rate of selective dissolution. The critical potential was rationalized by a potential-dependent surface mobility. Selective dissolution proceeds via surface migration of B exposing new A sites to solution. Simultaneously, B atoms aggregate to form crystallites. Transmission electron microscopy (TEM) studies of Au-Ag alloys provide strong support for this mechanism (8). The high surface mobility was attributed to partial ionization and solvation (*i.e.*, incipient oxidation) of gold. Forty and Rowlands (9) developed a quantitative treatment to describe the pitting or tunneling attack observed during massive dealloying. Similarly, Pryor *et al.* (10) portrayed dealloying as a short range process involving the collapse and recrystallization of B following the removal of A atoms. More recently, a percolation formalism (11), invoking surface diffusion, has been utilized to address this problem. Many of the morphological features observed by *ex situ* TEM and SEM studies, *e.g.*, clustering, smoothing, and local penetration phenomena, were favorably simulated.

To probe the mechanism of dealloying, Kaesche *et al.* (12, 13) used TEM and optical microscopy to examine the evolution of electrode morphology of a diverse series of alloys. Two limiting forms of behavior were revealed. Dealloying of "high-melting point" materials, *e.g.*, Cu-Pd and Cu-Au, occurred by nucleation and growth of microtunnels, while dissolution of "low-melting point" alloys, *e.g.*, SnIn, produced a homogeneous nonporous overlayer which was associated with the volume diffusion mechanism. Selective dissolution of ε-brass exhibited both morphologies and was considered to represent an intermediate case between "high- and low-melting point" materials. Thus, the dealloying mechanism appears to correlate to the "melting-point" of the alloy, presumably by correspondence with the magnitude of the diffusion coefficient.

In spite of this growing body of knowledge, there is currently no model that successfully describes the relationship between alloy composition and E_c. Information on the precise composition and morphology of the B-enriched blocking layer would be useful toward resolving the nature of the breakdown process associated with E_c.

Part of the difficulty associated with understanding dealloying phenomena has been the lack of appropriate tools for examining the evolving interface. *In situ* scanning tunneling microscopy (STM), with its attendant high spatial resolution and real-time capability, offers a means by which such electrochemical processes may be studied. A recent review of this technique is available (14). In this report, *in situ* STM is utilized to address the nature of the critical potential associated with dealloying of Cu₃Au.

The Cu-Au system was investigated because gold dissolution does not occur at the potentials associated with dealloying (5). Consequently, the measured current can be attributed solely to the dissolution of copper (5, 15). Furthermore, the electrochemistry of the constituent elements and the metallurgy of the copper-gold system are

well understood. At temperatures above 410°C, Cu-Au alloys form a fcc solid solution over the entire concentration range. At lower temperatures, however, a variety of ordered intermetallic structures are possible. Thus, by appropriate heat-treatment, Cu₃Au provides an additional opportunity to investigate the effects of ordering on electrochemical behavior. Curently, there are conflicting results concerning this matter (15-17).

Experimental

Cu₃Au was prepared by vacuum melting appropriate quantities of 99.999% Cu and 99.99% Au in an alumina crucible. The ingot was cold rolled into plate form and then sliced into specimens, $0.6 \times 0.6 \times 0.1$ cm. These specimens were heat-treated at 625°C, in vacuum sealed quartz ampuls, for approximately 144 h. One-half of the specimens were then quenched in ice water, yielding disordered Cu₃Au. The remaining specimens were ordered by cooling in a controlled manner over a six day period (380°C for 24 h, 330°C for 24 h, 280°C for 96 h). X-ray powder diffraction confirmed the respective crystal structures, as shown in Table I ($a_{ordered}$ = 3.754 Å, $a_{disordered}$ = 3.762 Å). A comparison of the measured and calculated diffraction peak intensities indicate a random distribution of crystal orientations within each sample. The structure factor calculations considered the multiplicity of diffracting planes and the Lorentz polarization factor (18).

Conventional electrochemical experiments were performed in a three-electrode cell held at 30°C. The working electrodes were prepared by first coating the specimens with a thin layer of Amercoat 90-High Performance Epoxy (Ameron Protective Coatings Division) to prevent crevice artifacts. These electrodes were then embedded in Epon 828/TETA Epoxy (Miller-Stephenson Chemical Co., Inc.) and cured at 75°C for 3 h. The electrodes were mechanically polished with γ-Al₂O₃ to a 0.05 μm finish immediately prior to any electrochemical experiments. A platinum counterelectrode and a saturated mercurous sulfate reference electrode (SSE) were utilized for all experiments

$$E_{SSE} = E_{SCE} - 0.4 \text{ V} = E_{SHE} - 0.64 \text{ V}$$

All solutions were prepared from Millipore (18 MΩ) water and analytical grade reagents: H₂SO₄ (<0.1 ppm Cl⁻), Na₂SO₄ (<0.0003% Cl⁻), HClO₄ (<0.001% Cl⁻), NaClO₄, HCl, NaCl.

Table I. X-ray diffraction data.

Ordered				Disordered			
$d(a)$	(hkl)	I_{meas}/I_{max}	I_{calc}/I_{max}	$d(A)$	(hkl)	I_{meas}/I_{max}	I_{calc}/I_{max}
3.743	100	22.5	35.4	2.168	111	100	100
2.648	110	22.9	30.0	1.879	200	94	47.6
2.163	111	100	100	1.329	220	56	29.3
1.876	200	62.7	48.6	1.134	311	64	35.6
1.678	210	19.3	16.3	1.084	222	20	11.2
1.531	211	23.9	12.2	0.940	400	23	7.6
1.326	200	48.1	29.2				
1.251	221	17.4	8.3				
	300						
1.188	310	14.4	5.4				
1.132	311	44.2	35.7				
1.083	222	17.9	10.8				
1.040	320	14.2	4.0				
1.004	321	19.6	7.6				
0.938	400	17.8	7.3				
0.910	410	19.1	8.0				
	322						

Disordered   **Ordered**

○ gold atom
● copper atom
◑ "average" gold-copper atom
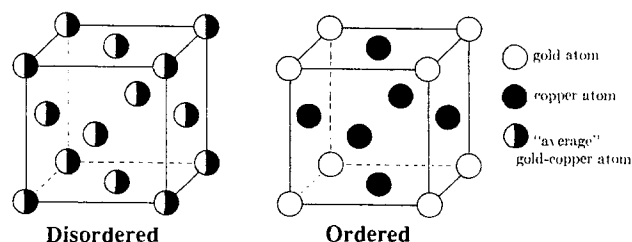
Details on the design, construction, and operation of the STM may be found elsewhere (19, 20). The STM tip was formed by etching a 125 μm diam Pt-Ir wire in a solution of saturated CaCl₂ (60% by volume, H₂O 36%, and HCl 4%) against a carbon rod at 20 V rms (21). The Pt-Ir tips were then partially encapsulated in soft glass, leaving a small exposed area around the tip. The electrochemical potential of the tip and substrate were independently controlled by a bipotentiostat. The tip potential was held in the double layer regime of platinum, $E = -0.2$ V. This gave a background faradaic current of <0.1 nA. The tunneling current was set 0.5 nA above the faradaic background. An STM image could be obtained in approximately 1 min. The STM experiments were performed at room temperature with the electrolyte exposed to the atmosphere.

Results

Overview of polarization behavior.—The electrochemical characteristics (log[i] vs. E) of Cu₃Au, copper, and gold in deaerated sulfate solutions are shown in Fig. 2. The dissolution of copper exhibits a linear log[i] vs. E plot (Tafel kinetics) with a slope of ca. 40 mV/dec. Copper dissolves by two consecutive electron transfer reactions, with the first step much faster than the second (22, 23)

$$Cu = Cu^+_{aq/ads} + e^- \quad \text{(fast)} \quad [1]$$

$$Cu^+_{aq/ads} = Cu^{2+}_{aq} + e^- \quad \text{(slow)} \quad [2]$$
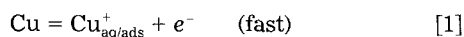
The relative importance of adsorbed vs. solvated Cu^+ is still an unresolved issue. Nevertheless, analytical treatments yield Tafel slopes ranging from 30 to 40 mV/dec. The low current (<0.5 μA/cm²) region of the curve for gold corresponds to the reduction (−0.6 V to −0.3 V) and oxidation (−0.3 V to +0.5 V) of solution impurities. The inflection of the curve at +0.5 V represents the onset of hydrous oxide formation, as revealed by cyclic voltammetry.

The potentiodynamic curve for Cu₃Au can be divided into three regimes. From the open-circuit potential to −0.4 V, the rate of dissolution increases with potential. This is attributed to oxidation of copper from surface sites of low coordination, i.e., kink sites. At −0.4 V, the current reaches a local maximum complemented by a significant level of electrochemical noise. As the surface becomes enriched with gold, the rate of dissolution decreases

$$Cu_3Au \rightarrow 3Cu^{2+} + Au + 6e^- \quad [3]$$
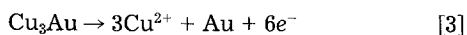
reaching a minimum at approximately −0.1 V. A current density of 1 μA/cm² corresponds to the removal of 0.2% of a monolayer equivalent of copper per second. Thus, the en-
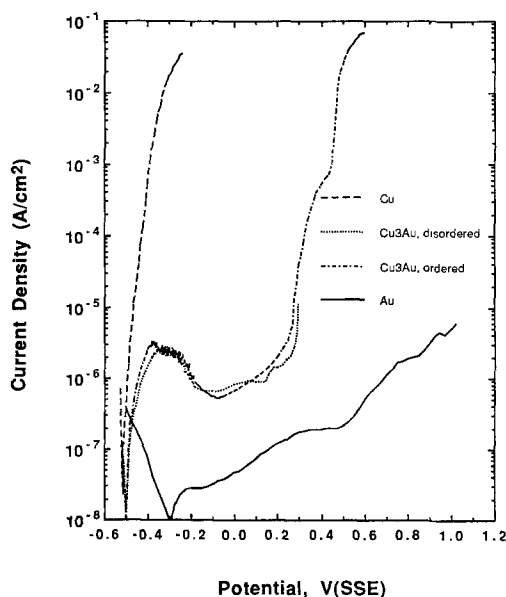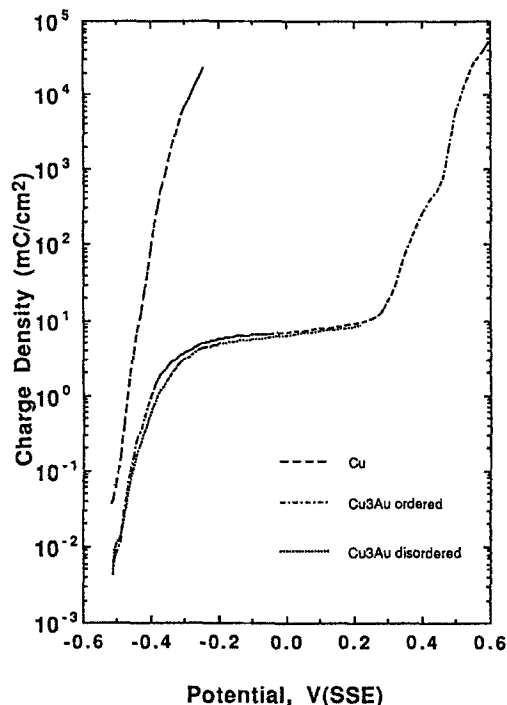
Fig. 3. The charge consumed during potentiodynamic polarization (chronocoulometric analysis of Fig. 2) of ordered and disordered Cu₃Au, and Cu in 0.01M H₂SO₄ + 0.99M Na₂SO₄ (pH = 2.8, T = 30°C, deaerated with argon, scan rate = 0.1 mV/s.)

richment of gold significantly blocks this reaction. At more positive potentials, the current increases slightly until a significant rise becomes apparent as the potential exceeds 0.3 V. The critical potential, E_c, corresponds to ca. 0.25 V. Above this potential the rate of dealloying increases rapidly. This is associated with the formation of a fine, highly porous surface structure. After extended anodization at high potentials, $E > E_c$, this sponge may be easily imaged by scanning electron microscopy. Massive dealloying also leads to parting of the grain boundaries. This may be ascribed to relaxation of the internal stress, which accompanies the selective removal of copper, or alternatively, the dissolution of the grain boundaries which is accelerated by segregated impurities. In contrast to other reports (15-17), no difference in the critical potential was observed between ordered and disordered Cu₃Au.

The i-E curve for copper and Cu₃Au was integrated over time to obtain the charge associated with the various polarization regimes. Assuming a uniform dissolution process, the charge can be converted into the quantity of copper removed such that 0.43 mC/cm² corresponds to the dissolution of a monolayer equivalent of copper from Cu₃Au. Three regimes of behavior are noted in Fig. 3. The low overpotential region, $E < -0.4$ V, corresponds to the passage of submonolayer to ca. 1 mC/cm² of charge. Globally speaking, this corresponds to the dissolution of ca. 1-3 layers of copper which is equivalent to a coverage of the electrode by up to a monolayer of gold. This leads to the passivation of the electrode, although a small but measurable dissolution process continues to operate. The protective passive layer breaks down at +0.25 V. This occurs after the passage of charge of ca. 10 mC/cm² equivalent to the removal of ca. 25-30 layers of copper which results in a gold overlayer of ca. 10 monolayers.

A deeper understanding of the current-potential behavior of Cu₃Au requires careful specification of the morphology and composition of the evolving interface. This is particularly important for potentials ranging from −0.1 V to E_c. Inspection of the i-E curve indicates that the current increases slowly with potential in this domain. At present, it is unclear if this increase is attributable to copper oxidation or to the oxidation of solution impurities. This second description is identical to that utilized for the gold electrode ($E < 0.5$ V), but with the surface area of Cu₃Au en-

Fig. 2. Potentiodynamic polarization behavior of ordered and disordered Cu₃Au, Cu and Au in 0.01M H₂SO₄ + 0.99M Na₂SO₄. (pH =2.8, T = 30°C, deaerated with argon, scan rate = 0.1 mV/s.)
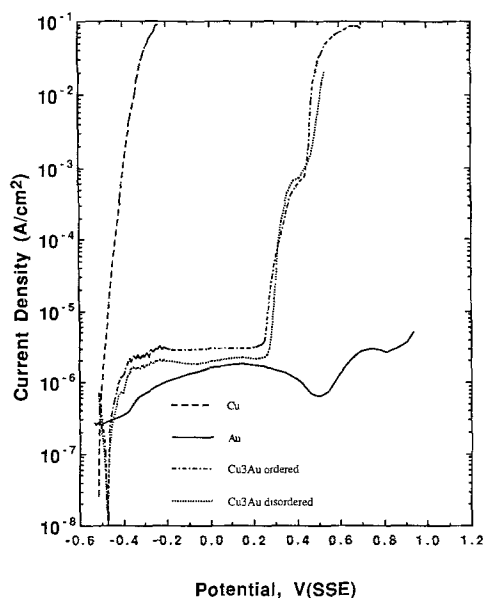
Fig. 4. Potentiodynamic polarization behavior of ordered and disordered Cu₃Au, Cu and Au in 0.01M H₂SO₄ + 0.99M Na₂SO₄. (pH = 2.8, T = 30°C, deaerated with hydrogen, scan rate = 0.1 mV/s.)

hanced by an order of magnitude due to transient dealloying of copper. To explore this matter, the response of these electrodes to the presence of dissolved hydrogen gas was investigated. The proton/hydrogen couple was utilized, because the rate of reaction is controlled by interfacial charge transfer and consequently represents a sensitive measure of the active area of the electrode. In Fig. 4, the $\log[i]$-E curve for a hydrogen-purged solution is shown. For potentials up to E_c, the behavior of Cu₃Au and gold are essentially indistinguishable. Thus the active surface area of Cu₃Au is similar to that for gold. Transient dealloying leads to no more than a doubling of the roughness factor. This indicates that the current density measured for Cu₃Au in an argon-purged solution is attributable to the oxidation of copper.

Cyclic voltammetry and UPD phenomena.—Cyclic voltammetry of Cu₃Au revealed useful information concerning the evolution of the surface during dealloying. A typical voltammogram is shown in Fig. 5. The electrode was pre-
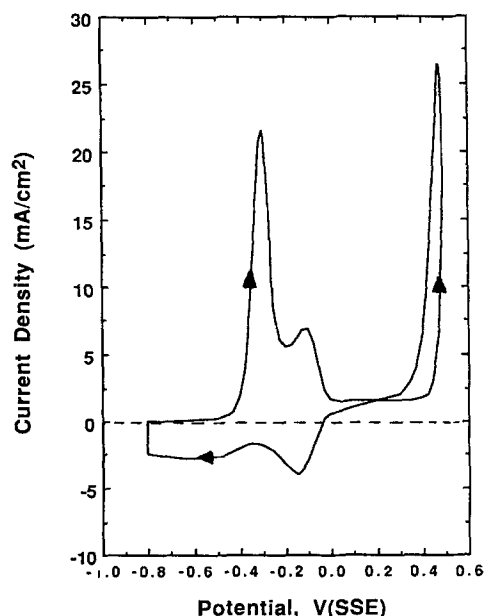
Fig. 5. Cyclic voltammogram of disordered Cu₃Au in 0.01M H₂SO₄ + 0.99M Na₂SO₄. (pH = 2.8, T = 30°C, deaerated with argon, scan rate = 200 mV/s).
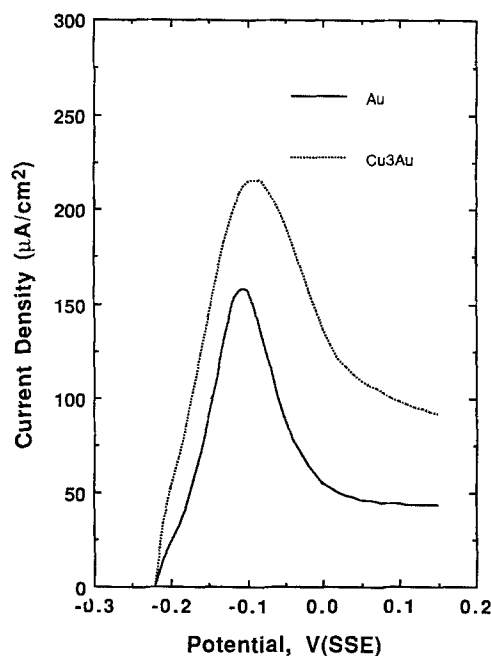
Fig. 6. Stripping of upd copper from Cu₃Au and Au. Cu₃Au was dealloyed by polarizing at 0.150 V for 1 h. Upd was performed by polarizing each electrode at −0.222 V for 1 min in 0.2 mM CuSO₄ + 0.01M H₂SO₄ + 0.99M Na₂SO₄. (Scan rate = 200 mV/s.)

polarized in the passive domain producing a gold-enriched surface. Sweeping the potential to positive potentials led to a rapid increase in anodic current at $E > 0.4$ V, producing a large quantity of Cu²⁺ ($E > E_c$). Upon cycling the potential between +0.5 V and −0.8 V, a pair of (cathodic/anodic) peaks develop at ca. −0.125 V. These peaks are due to the underpotential deposition (upd) and oxidation of copper from the gold-enriched dealloyed surface. The peak potential agrees favorably with previous results concerning the upd of copper on gold (24). At more negative potentials, deposition of bulk copper occurs followed by the corresponding stripping peak (ca. −0.30 V) on the reverse scan.

The observation of upd has two important consequences. For potentials more negative than −0.1 V, upd of copper on the gold-enriched regions of the alloy surface is possible. Therefore, the corresponding charge must be considered when analyzing data from experiments such as chronoamperometry. Second, the phenomenon of upd provides a useful probe for investigating the chemical nature of the gold-rich blocking layer. Upd corresponds to the formation of up to a monolayer of material (Cu) on a foreign substrate (Au) and is thus a highly sensitive *in situ* probe of the substrate surface area (peak area) and composition (peak potential) (24). This method of *in situ* "surface analysis" is superior to conventional *ex situ* probes (AES, XPS, etc.) by virtue of its highly surface specific nature. In particular, this technique circumvents the difficult and ambiguous analysis that follows from a consideration of the mean-free path of Auger and photoelectrons.

Upd of copper was utilized to determine the nature of the surface of Cu₃Au following transient dealloying immediately below the critical potential, $E < E_c$. A freshly polished electrode was held at 0.150 V for 1 h. Deposition of Cu from a 0.2 mM Cu²⁺ solution was performed by stepping the potential to −0.222 V and after 1 min sweeping the potential in the positive direction; stripping of upd copper was monitored. A similar experiment was performed on a pure gold electrode (with the dealloying procedure, *i.e.*, polarization at 0.150 V, omitted). As shown in Fig. 6, the peak potential of the stripping waves were about the same for gold and Cu₃Au. Thus, dissolution of Cu₃Au leads to the formation of a blocking layer of essentially pure gold. Integration of the stripping peaks indicated that the surface coverage of gold sites for upd is greater on anodized Cu₃Au (ca. 0.230 mC/cm²) than on the

A.

B.
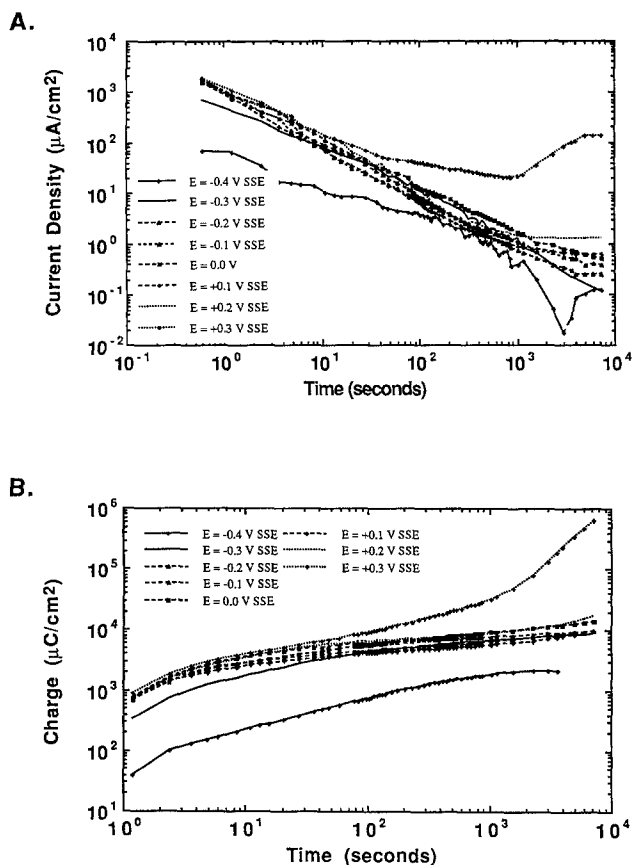
Fig. 7. (A) Chronoamperometric results for ordered Cu₃Au. Each transient was obtained for a freshly polished electrode. The initial potential was −0.5 V. (B) Charge density transients obtained by integration of the chronoamperometric results.

A.

B.

Fig. 8. (A) Chronoamperometric results for ordered Cu₃Au. A single electrode was progressively polarized by stepping the potential, once every hour, from −0.5 V to 0.3 V. (B) Charge density transients obtained by integration of the chronoamperometric results.

gold electrode, (*ca.* 0.125 mC/cm^2). This gives an increase in the roughness factor of *ca.* 2, in agreement with the results for hydrogen oxidation shown in Fig. 3.

Chronoamperometry.—Chronoamperometry was utilized to investigate the kinetics of formation and breakdown of the passivating gold overlayer. The current decay at a given potential was measured and integrated to obtain the corresponding charge. Assuming uniform dissolution, the anodic charge can be converted into the number of layers of copper removed, based on a charge of 0.43 mC/cm^2 corresponding to the dissolution of a monolayer equivalent of copper from Cu₃Au.

Two different sequences of experiments were performed. The first, shown in Fig. 7, involved stepping the potential of a freshly polished electrode from −0.5 V to a value of interest. For the −0.2 V to 0.2 V transients, the current decreased rapidly with time due to the progressive enrichment of gold at the interface, which blocked the further dissolution of copper. The transients were essentially independent of potential. The measured decay rate gives a slope of *ca.* −1 which is in agreement with experimental results for Cu₇₀Au₃₀ (25). The solid-state diffusion model of Pickering and Wagner (5), as well as the surface diffusion model of Forty and Rowlands (9), predicts a slope of −0.5 for these transients. More recently, Laurent and Landolt (26) have successfully applied a four-parameter model, involving both surface and bulk diffusion, to describe current transient at subcritical potentials ($i \propto t^{-m}$ where $0.8 \le m \le 1.0$). After 1000 s, the charge passed corresponded to the removal of 13 to 21 layers of copper. The exact quantity of charge did not appear to be a function of potential, although greater precision may reveal a slight dependence. Combined Auger and transient studies found the enrichment of gold to be a direct function of the amount of charge passed (25, 26). The −0.3 V transient initially has a slope of −0.5 which changed to −1 after 20 s, coinciding with the oxidation of *ca.* five equivalent layers of copper.
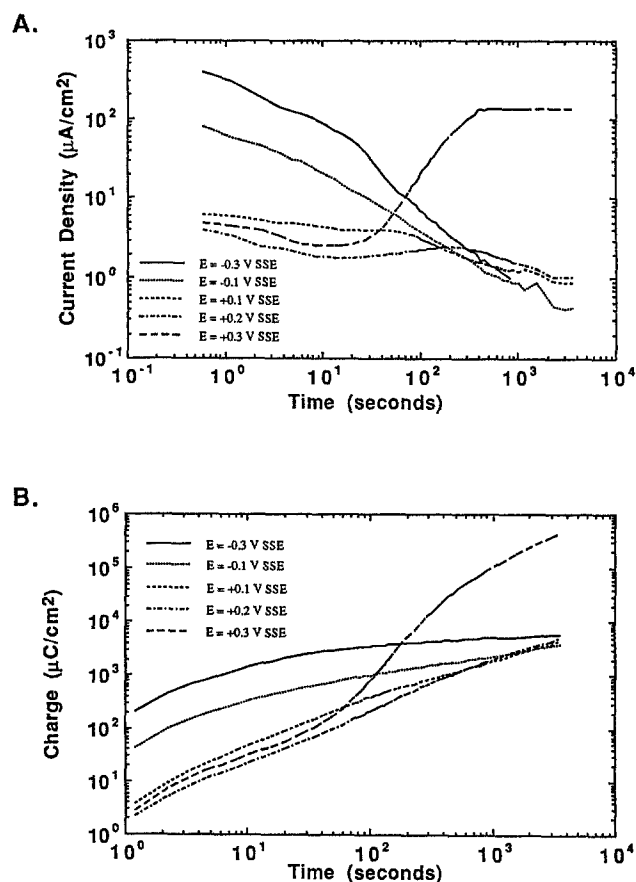
At −0.4 V the initial current density was much lower in magnitude and the slope was −0.6. A monolayer equivalent of copper was removed after 36 s. After extended polarization, 3000 s, the surface was covered by about one monolayer of gold and the current changed sign with a net cathodic process being measured. Although it is not apparent in Fig. 7, a significant component of electrochemical noise was associated with the −0.4 V and −0.3. V transient. A comparison of these results with the polarization curve given in Fig. 2 suggests that the evolution of the transients at −0.4 V and −0.3 V corresponds to a regime where the details of the copper dissolution reaction are important to the measured kinetics. The electrochemical noise associated with the −0.4 and −0.3 V transients may be attributed to a coupling of the copper dissolution with the random unblocking of sites of copper oxidation by the diffusion of gold atoms. Upd of copper may also play a role in transients for $E < 0.1$ V, however, the total contribution would be less than 0.23 mC/cm^2.

When the potential was stepped above the critical potential to 0.3 V, the transient initially exhibited the same decay rate. However, after 10 s the rate of passivation decreased and after 1000 s the current began to increase. The first indication of breakdown occurred after the passage of 6 mC/cm^2, corresponding to the removal of 14 layers of copper. This charge or incubation time is characteristic of nucleation and growth phenomena.

The second series of chronoamperometric experiments involved progressively stepping the potential of the same electrode to more positive values. In Fig. 8 the current and charge density transient are given for five potentials. The first potential step was from −0.5 V to −0.3 V. In agreement with the previous experiment, the current decayed with a slope of *ca.* −0.5, but after 20 s (equivalent to 2 mC/cm^2 or *ca.* five layers of copper removed from Cu₃Au) the slope changed to *ca.* −1. After 1 h the potential was stepped to −0.1 V. A similar transient was obtained, al-
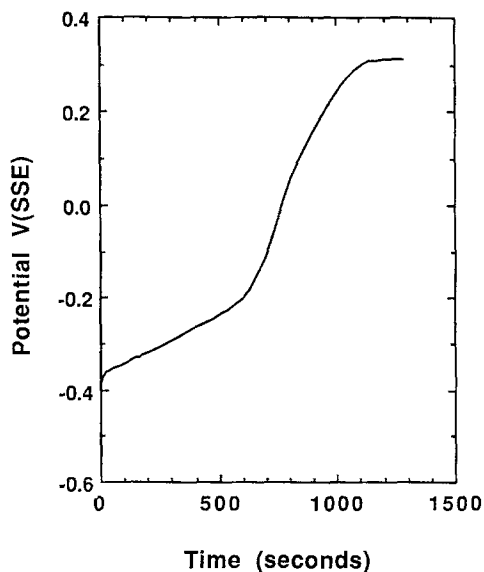
Fig. 9. Chronopotentiometry for disordered Cu₃Au for an applied current density of 10 μA/cm².

Fig. 10. A normalized summary of chronopotentiometry at a variety current densities.

though the magnitude of the current in the first segment was significantly lower than the first transient. The transition in this instance occurred after 7 s (0.22 mC/cm² or 0.5 monolayer of copper). Upon then stepping the potential to 0.1 V, the initial current was quite low <10 μA/cm² and decayed very slowly with time. After 80 s (0.3 mC/cm² or ca. 0.7 monolayer), a transition in the slope to −1 occurred, as with the previous transients. When the potential was then stepped to 0.2 V, the transient was initially quite similar to the previous ones, although the current was smaller in magnitude. After 20 s (0.04 mC/cm² or ca. 0.1 monolayer of copper), the current began to increase. A maximum was reached after 220 s (ca. 0.5 mC/cm² or one monolayer of charge) and then the current continued to decay. After stepping to 0.3 V, which is above the critical potential, for a short time the current transient was similar to that of the two prior transients. However, after 20 s (0.05 mC/cm² or 0.1 monolayer of copper), the current began to increase continuously. This is in qualitative agreement with the results reported for Cu₈₇Au₁₃ (15). As with the first set of chronoamperometric experiments, the initial portion of the transient, for $E > E_c$, corresponds to an induction or nucleation time for breakdown of the passive overlayer. This incubation time decreases as $\{E - E_c\}$ is increased (15). In the first set of experiments the removal of 14 monolayers of copper was necessary before breakdown occurred. In contrast, the dissolution of 43 monolayers of copper preceded breakdown in the progressive polarization experiment, and 30 monolayers were dissolved in the potentiodynamic experiment. These differences indicate that the nucleation process depends on the total duration of the experiment as well as charge, *i.e.*, on aging effects.

Chronopotentiometry.—When an anodic constant current pulse of 10 μA/cm² was employed to dealloy Cu₃Au, three regimes of behavior could be distinguished (Fig. 9). In the first region, the potential increased with time as copper was selectively dissolved and the surface became enriched in gold. A transition occurred at 550 s which is attributed to the depletion of easily oxidized copper sites. After 1100 s a steady-state potential was reached which corresponded to that expected from the potentiodynamic curve (Fig. 2) for a current density of 10 μA/cm². Results obtained with other current densities were similar, when these were normalized by plotting the potential as a function of the charge passed (Fig. 10). The rapid transition through the passive region was almost independent of the applied current density. The sharp rise began after ca. 2 mC/cm² (corresponding to a monolayer of gold) and was typically complete after the dissolution of 5-8 mC/cm² (ca. 11-18 equivalent layers of copper). However, the initial stage of dealloying was sensitive to the applied current
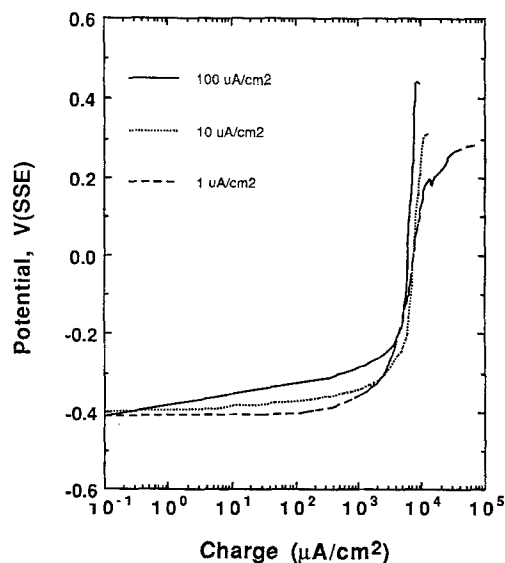
density. For higher dealloying rates, blocking by the gold-enriched interface was more important. This suggests that the number of active sites for copper dissolution is a function of time. A surface which is initially blocked reorganizes with time leading to the exposure of fresh copper sites.

This surface relaxation process was further investigated by performing chronopotentiometry with periodic interruption of the applied current. Typically, the current was interrupted for 30 s and then reapplied, as shown in Fig. 11. For potentials below E_c it took tens of seconds for the potential to recover the value obtained prior to interruption. This is attributed to reordering of the surface (and possibly upd of copper, if $E < 0.0$ V) during the interruption, which leads to a higher density of oxidizable copper sites. For potentials above E_c, interruption and reapplication of the current led to the potential increasing to a value greater than that before interruption, and then, after 10-100 s, decaying to the steady-state potential anticipated from the potentiodynamic curve. This phenomenon is probably related to the incubation or nucleation time observed in chronoamperometric studies. Thus, the dissolution of copper depends on the surface mobility of gold, *i.e.*, unblocking of copper sites.

In situ scanning tunneling microscopy.—*In situ* STM was utilized to investigate the evolution of the alloy interface over a range of potentials. In agreement with potentiodynamic polarization studies, three different regimes of behavior were noted. At low overpotentials, oxidation of low coordination copper sites occurred with the concurrent enrichment and clustering of gold. This reconstruction process results in passivation of the electrode, al-
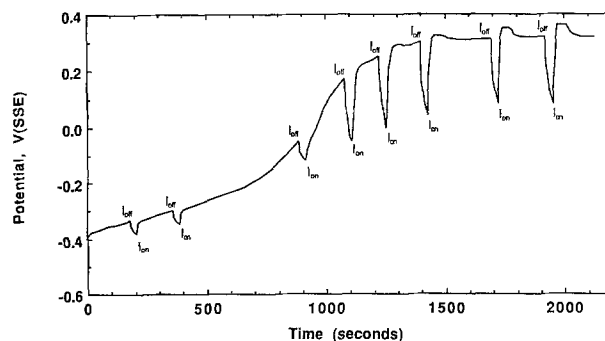
Fig. 11. Chronopotentiometry for disordered Cu₃Au at a curent density of 10 μA/cm². Relaxation of the interface was monitored by interrupting the applied current at various potentials.
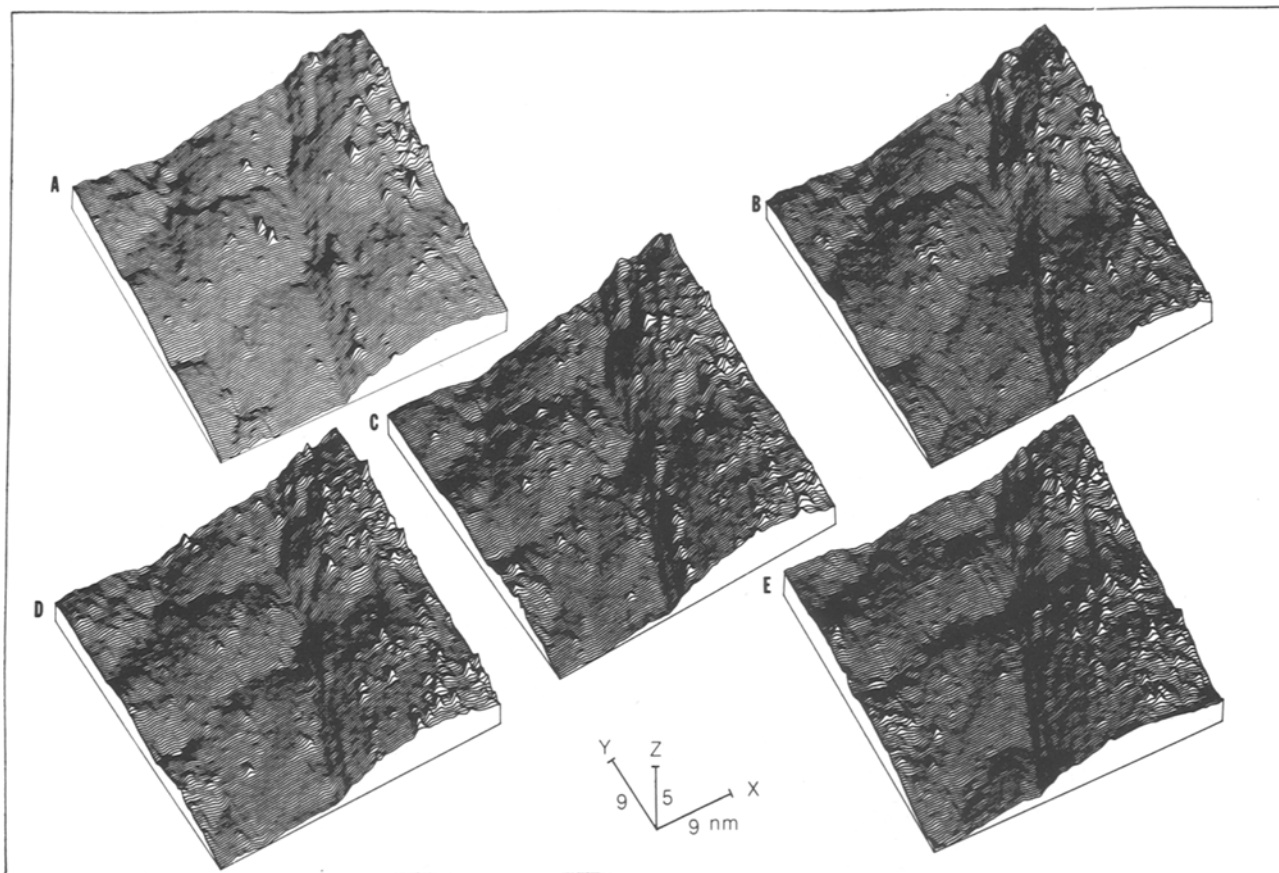
Fig. 12. A sequence of topographic, constant-current STM images of disordered Cu₃Au progressively held in the low overpotential regime: (A) −0.480 V for 2 min, (B) for 4 min, (C) at −0.450 V for 2 min, (D) for 4 min, (E) at −0.400 for 2 min.

though small areas of three-dimensional roughening were also observed. At still higher potentials, $E > E_c$, breakdown of the protective overlayer occurred, as signified by roughening of the electrode. Breakdown appears to spread from the localized regions of three-dimensional roughness that were apparent in the passive region, *i.e.*, $E < E_c$.

Low overpotentials.—In Fig. 12 a series of STM images are presented for an electrode polarized at low overpotentials. The sequence represents the same area as is evident from the characteristic markers visible in all the images, *i.e.*, the ledge or slip step passing almost vertically through the center of the image. In Fig. 12A several bumps or hills *ca.* 10 Å in height are apparent. Comparison with Fig. 12B indicates that these features grow and disappear with time. Various complementary electrochemical methods indicate that the dissolution of submonolayer quantities of copper occurs during the recording of these images. Therefore, we feel that these hill-like features represent the clustering of gold near the sites of copper dissolution. The hill-like clusters relax with time, reflecting the known mobility of gold and the tendency of the system to minimize its surface energy.

Stepping the potential from −0.480 V to −0.450 V leads to the continued activation of other sites of copper oxidation as demarked by the formation and smoothing of gold clusters. In Fig. 12C and 12D the active sites on the ledge are clearly shown. Further polarization of the specimen to −0.4 V leads to the activation of additional sites on the surface, particularly on top of the protruding ledge or slip step. Macroscopic observations previously indicated that dealloying occurs readily at slip bands (27).

Passive domain.—In Fig. 13 a series of STM images are presented following a potential step from −0.5 V to −0.35 V. The development of a rough structure was apparent following polarization at −0.35 V. This rough region grew laterally as a function of time and, after a few min-

utes, little additional growth was observed. Integration of the current transient from a corresponding experiment (Fig. 8) indicated that a maximum of five to ten monolayer equivalents of copper had been dissolved. The bulk of this charge was passed within the first few minutes of the transient. No substantial roughening of the surface would be anticipated after this time, consistent with the STM images. Further polarization at higher potentials in the passive region led to negligible alteration of the surface. This is supported by the chronoamperometric results which reflect the passage of insignificant quantities of charge upon progressive stepping of the potential in the low current regime, *i.e.*, the bulk of the charge is passed on the first potential step from open circuit, especially for $E > -0.3$ V (see Fig. 8).

The sinusoidally roughened domain shown in Fig. 12B and C represents the three-dimensional clustering of gold into islands at sites of extensive copper dissolution. A similar type of structure has been observed in a transmission electron microscopic (TEM) examination of a Cu-10%Pd alloy, as shown in Fig. 14. According to Kabius *et al.* (12) these "dissolution nuclei" appear to be tied to solid-state defects, such as dislocations. These nuclei may penetrate on the order of 50 Å beneath the surface. Consequently, a large portion of this region is inaccessible to the STM tip. Pickering *et al.* (15) have shown that the charge associated with transient dealloying in this potential range is a function of the defect density in the solid. The localized nature of the roughening attack, and its sensitivity to defect structures, suggests great caution is required in the interpretation of chronoamperometric data for the passive regime.

Critical potential.—Shown in Fig. 15 are STM images, when the critical potential was exceeded. The electrode was initially held at 0.0 V for 30 min, and then the potential was stepped above the critical potential (to 0.3 V). The image obtained after two min revealed several hill-like clusters of gold. The surface coverage of these hillock re-
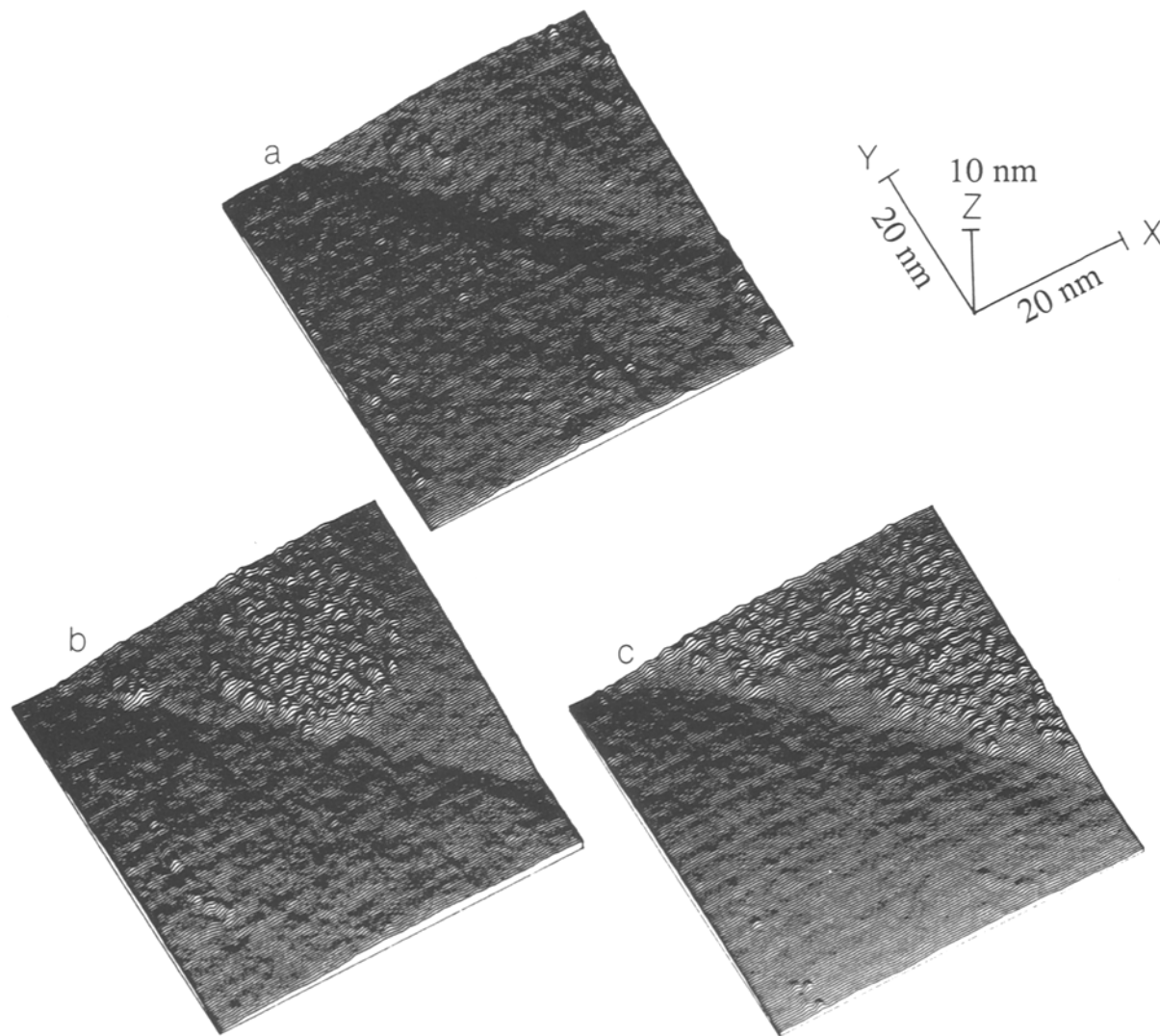
Fig. 13. Topographic, constant-current STM images of disordered Cu_3Au for a potential step into the passive region: (a) initial condition at −0.550 V for 4 min, (b) at −0.35 V for 2 min, (c) for 4 min.

gions increased with time. This is particularly apparent on the left-hand side of the image. The growth of these domains is consistent with the chronoamperometric results for $E > E_c$. As noted in Fig. 7, the increasing current associated with breakdown is preceded by an incubation period of *ca.* 30 s. The faradaic current then increases continuously until a steady-state value is attained in 8-10 min.

When the potential was increased to 0.4 V, the hill-like formations covered a larger fraction of the surface. Some of the hillocks were quite large compared with those observed at lower potentials. When the potential was reversed to below the critical potential, the hill-like features dissipated quite rapidly. This simple experiment demonstrates the remarkable surface mobility of gold associated with the dealloying process. The rapid nature of this process calls into question any detailed analysis of the dealloying problem performed by *ex situ* probes (*e.g.*, XPS, AES).

Influence of adsorption on dealloying.—The STM results indicate that the surface of the dissolving alloy undergoes significant reconstruction. This process must involve surface migration of gold. Consequently, adsorption phenomena should play a strong role in the dealloying process. This was investigated by examining the potentiodynamic behavior of Cu_3Au under conditions where adsorption phenomena on gold are relatively well understood. Polarization characteristics were monitored in acid solutions (pH = 2.8) of $1M$ ClO_4^-, SO_4^{2-}, and Cl^-. The electrochemical characteristics were essentially the same in sulfate and perchlorate media. In chloride solutions, however, the

critical potential, E_c, was reduced. The depression of E_c was a monotonic function of chloride concentration, as shown in Fig. 16. This implies that the surface coverage of chloride is proportional to the bulk concentration. The sulfate and perchlorate solutions contain trace chloride levels of ≤ 12 μM. Thus, in Fig. 16, the E_c value of 0.25 V corresponds to a one molar sulfate or perchlorate solution. It is likely that purification of the solution would lead to a further increase in the critical potential. The variation in the measured critical potential reported in the literature may be attributed to variation in the trace chloride content of the media employed (15). While chloride alters the mechanism of copper dissolution (22), this is of no importance at overpotentials as high as the critical potential. In a recent publication, Nichols *et al.* (28) used *in situ* STM to show that chloride, unlike sulfate or perchlorate, interacts strongly with a gold electrode, leading to a large increase in the mobility of gold atoms at step and kink sites. Several other researchers have also observed the rapid transport of gold in chloride media by STM (29-32).

It should also be possible for adsorption, *e.g.*, of thiols, to inhibit the transport of gold atoms. Alkylthiols bond strongly to gold surfaces through the sulfur atom (33). In addition to any electronic effects associated with the sulfur-gold bond, mass and steric hindrance associated with the alkyl chain could act to inhibit the surface mobility of gold. The potentiodynamic behavior of Cu_3Au and copper was investigated before and after treatment with $C_5H_{11}SH$. The electrodes were treated by immersion for 5-10 min in a solution of 0.1 ml $C_5H_{11}SH$ in 25 ml ethanol. The electrodes were then rinsed successively with ethanol and water prior
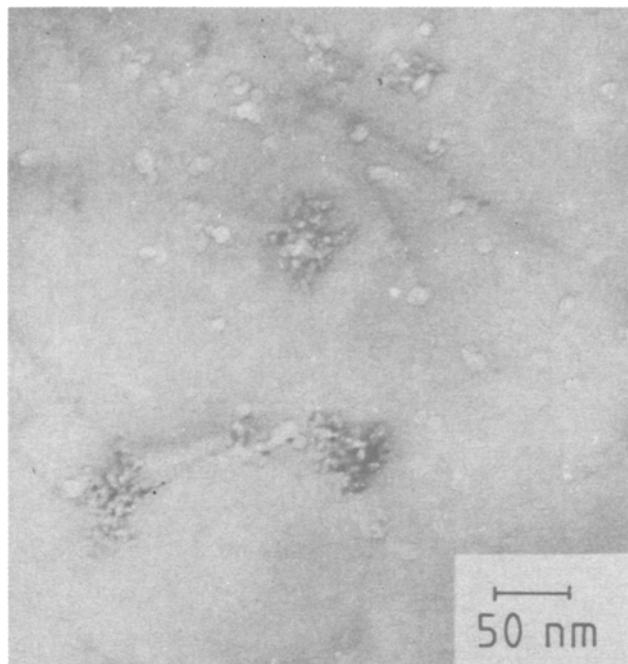
Fig. 14. A TEM micrograph of dissolution nuclei and dislocations on a $Cu_{90}Pd_{10}$ alloy polarized below the critical potential; taken from Kabius et al. (12).

to polarization in acidic sulfate solution. As shown in Fig. 17, such treatment did not inhibit the dissolution of pure copper. In contrast the polarization characteristics of Cu_3Au were significantly altered. The critical potential was increased by 150 mV, while in the region of active dissolution, a small inhibition of copper dissolution was apparent.

Since the dissolution of pure copper was largely unaffected by derivatization, these features may be attributable to the slowing or inhibition of the surface mobility of gold. In agreement with these observations, Alonso et al. (34) used electrodispersed gold electrodes to measure the effects of adsorption on the surface diffusion coefficient, D_s, of gold. In sulfate media, the adsorption of pyridine produced a significant decrease in D_s, whereas adsorption of chloride resulted in the opposite effect.

Discussion

A combination of *in situ* STM and other electrochemical methods has demonstrated the importance of Au surface mobility and reconstruction in the dealloying of Cu_3Au. Dissolution at low overpotentials, *i.e.*, $E < -0.4$ V, involved submonolayer quantities of charge. STM suggested the aggregation of gold atoms near sites of copper dissolution. This may be envisioned as a two-dimensional process following the kink-ledge-terrace model of dissolution and passivity. A schematic of this process is given in Fig. 18. Progressive dealloying depends on the unblocking of active copper sites by the movement of gold atoms. Evidence of this time-dependent process was also found in chronopotentiometric experiments. For a given charge, the electrode polarized more rapidly as the applied current density was increased. Similarly, derivatization of Cu_3Au with $C_5H_{11}SH$ inhibits the dissolution of copper by slowing down the surface migration of gold.

As the potential is increased, an additional quantity of copper is removed from the surface leading to the formation of a passivating gold-rich layer. Upd experiments indicate that the outer portion of this overlayer is pure gold. A more refined application of upd would entail studying the deposition of a foreign ion such as Pb^{2+}. The deposition potential of Pb^{2+} is sensitive to the identity of substrate atoms, thus allowing the possibility of identification of copper as well as gold sites (35). This experiment would offer the added capability of monitoring the complete
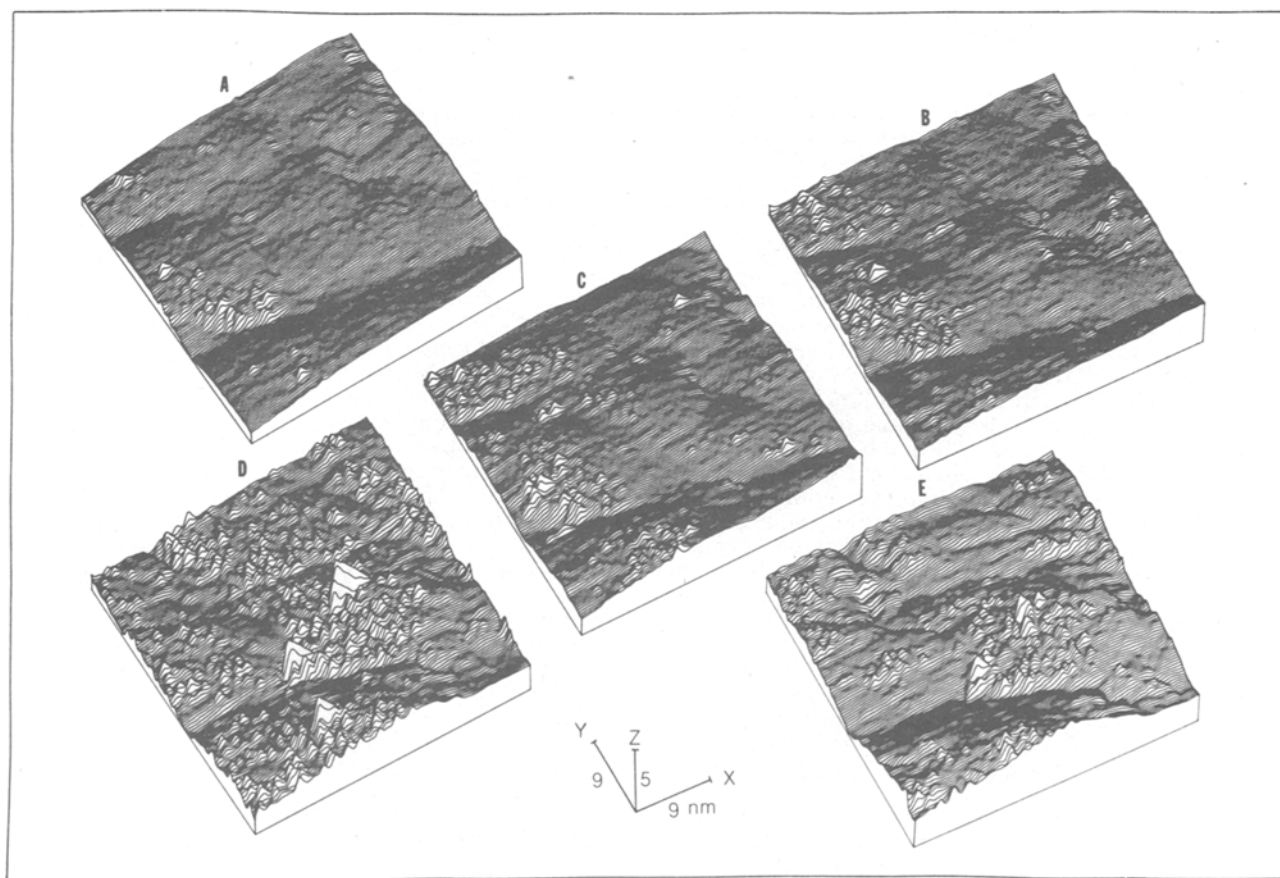
Fig. 15. A sequence of constant-current STM images of disordered Cu_3Au following polarization above the critical potential, $E_c = -0.250$ V; (A) at 0.0 V for 30 min, (B) at 0.3 V for 2 min, (C) for 4 min, (D) at 0.4 V for 4 min (E) reverse potential step to 0.0 V after 4 min.
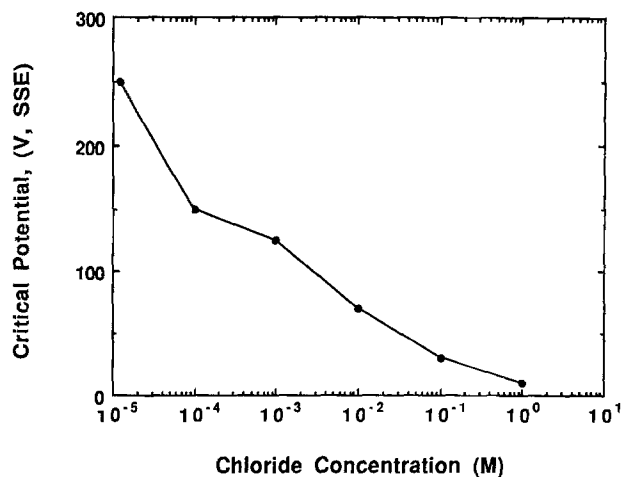
Fig. 16. The influence of chloride ion adsorption on the critical potential, E_c. The E_c values were determined by potentiodynamic polarization at 1 mV/s in argon deaerated solution (pH 2.8). The total anion concentration was maintained at molar strength, *i.e.*, xM Cl$^-$ + yM SO$_4^-$ where $x + y = 1$.

Fig. 18. Schematic of selective dissolution of a binary alloy by a surface migration controlled mechanism [adapted from Ref. (1)].

dealloying process in real time, *i.e.*, the enrichment of gold as well as the removal of copper. (A flow cell would be required to avoid complications associated with upd of copper.)

At potentials in the passive domain localized regions of significant roughness were observed by STM. In agreement with TEM results of Kabius *et al.* (12), these features were identified as dissolution nuclei. These domains were correlated to sites where dislocations intersect the surface (12). The relatively large size of the dealloyed region may be attributed to enhanced transport of copper in the dislocation pipe and migration of the dislocation due to oxidation of copper from the core, *i.e.*, dislocation climb. By analogy, this is related to the dealloying process associated with diffusion-induced grain boundary migration (36). The hill-like structures in the STM images are essentially pure gold, and this network extends several tens of angstroms into the solid beyond the apparent solid-solution interface. In contrast to the two-dimensional dealloying process seen at lower potentials, complete smoothing of these hill-like

Fig. 17. Potentiodynamic polarization behavior of disordered Cu₃Au and Cu, before and after derivitization with C₅H₁₁SH (0.01M H₂SO₄ + 0.99M Na₂SO₄, pH = 2.8, T = 30°C, deaerated with argon, scan rate = 1 mV/s).

features does not occur on the time scale of the STM experiment. This does not preclude such coarsening phenomena but rather represents a limitation of STM for monitoring deep holes or what is now a three-dimensional process. The highly localized nature of these regions calls for great caution in dealing with chronoamperometric results. Traditionally, these transients have been interpreted in terms of global surface processes which is clearly not the case. Transients in the passive domain indicate that on the order of 15 layers of copper are removed globally. This is equivalent to the surface being covered by five layers of gold. A more likely situation would consider a significant portion of this charge attributable to the dissolution nuclei. Furthermore, the low currents observed in the passive domains may be due to the slow growth of these nuclei. STM experiments over a larger area and longer time scale will be needed to resolve this point.

As the potential is raised above the critical value, the rate of dealloying increases precipitously. STM reveals that this is associated with a roughening transition which largely occurs by growth of the three-dimensional dissolution nuclei. Chronopotentiometry and chronoamperometry indicate that the growth or reactivation of the nuclei is associated with an incubation time. The incubation time was a function of $\{E - E_c\}$.

Gladen *et al.* (13) envisage the nucleation process as the formation of vacancy clusters in the passive overlayer. For growth to occur, the nuclei must be larger than a critical size. Thus, the critical potential corresponds to the formation and growth of clusters exceeding this critical size. The critical size parameter is a function of potential. The potential dependence of the surface tension of the gold passive layer in combination with the surface diffusion coefficient would be the determining factors in this model. In support of this, Nichols *et al.* (28) have noted that significant changes in the surface topography of gold take place in the double layer charging region. These alterations occur more rapidly as the potential is increased. In a similar vein, the role of electrocapillary action in the anodic breakdown of passive films on metals has been examined by Sato (37).

The rapid dissolution of copper from Cu₃Au, at high overpotentials, leads to a highly defective surface such that solid-state diffusion through this layer may also contribute to the overall dealloying process. However, as shown in Fig. 16 and 17, the dependence of E_c on adsorption phenomena points to a surface process being rate limiting. Galvele (38) has reviewed the literature on the effects of impurities on the surface diffusion of metals in UHV. Surface mobility was found to increase if the melting temperature of the corresponding absorption compound was less than that of the metal. The effect of chloride on E_c is in agreement with this formulation, while that for the derivitized electrode is not. This indicates that the differing solubilities (*i.e.*, tendency for complexation) of AuCl or AuCl₃ (very soluble) *vs.* Au₂S or Au₂S₃ (insoluble) must also be considered when dealing with surface mobility in electrode/electrolyte systems.

After extended dealloying, reversing the potential to below E_c leads to a rapid smoothing of the surface. This further demonstrates the dramatic mobility of gold on the dealloyed surface. Pickering (39) observed similar "smoothing or aging" effects for $Cu_{90}Au_{10}$ by capacitance measurements. Similarly, Tomsett *et al.* (40) have reported coarsening of the porous copper sponge layer formed on CuAl alloys.

Relevance to stress corrosion cracking (SCC).—Accumulating evidence suggests that there is a strong link between dealloying phenomena and stress corrosion cracking (2, 3, 41). Copper-gold alloys have been utilized as a model system for examining this connection (3, 41, 42). Cracking is often associated with conditions that lead to the profuse surface roughening and porosity. The notion that the critical potential, E_c, defines the transition from a planar to a porous interface indicates a link between E_c and SCC susceptibility (2). However, Lichter *et al.* (3, 42) have recently shown that cracking can occur at potentials significantly below E_c. The three-dimensional dissolution nuclei observed by STM, for $E < E_c$, represent plausible sites for the initiation of SCC. Thus, the link between three-dimensional dealloying and SCC is reinforced. Additional data (3, 42) show that the rate of crack growth is a monotonic function of potential, suggesting a relationship between crack growth and the surface mobility of gold. This is consistent with a recently proposed SCC model based on surface mobility (38).

In contrast, Kelly *et al.* (43) reported that nanoporous regions can nucleate brittle cracks in the substrate but aging of the as-formed sponge leads to a loss of this ability. Similarly, Fritz *et al.* (44) determined that crack growth, initiated in a dealloyed layer produced above E_c, can be terminated by stepping the potential below E_c. The analogous STM experiment demonstrates that significant surface reconstruction occurs when the potential is stepped below E_c. Thus, it is clear that the dynamics of formation and coarsening of the nanoporous layers is of great importance to resolving the connection between dealloying and SCC phenomena.

SCC is often investigated by monitoring current transient from fresh metal surfaces obtained by scraching techniques (42, 45). These macroscopic experiments attempt to correlate the measured electrochemical currents with the rate of nucleation and growth of cracks. However, the highly localized attack ($E < E_c$) revealed by STM suggests great caution must be used in transcribing the measured transients from current to current density.

Conclusions

The utility of *in situ* STM analysis of corrosion processes such as dealloying has been demonstrated. Three different regimes of behavior were noted for the dealloying of Cu_3Au. At low overpotentials, clustering of gold atoms occurs near sites of copper dissolution. The formation and smoothing of these clusters was monitored in real time, demonstrating the highly mobile nature of surface gold atoms. At higher potentials, the surface is passivated by the enrichment of gold, however, there exist small localized domains of three-dimensional roughness which may be correlated to extended dealloying catalyzed by bulk solid-state defects. These regions may act as crack initiation sites for SCC. When the potential exceeds a critical value, E_c, global surface roughening occurs. Correlation with chronoamperometry and chronopotentiometry demonstrates that this transition is a nucleation and growth process. In this regime, the dissolution of copper depends on the migration of gold exposing fresh sites. The mobility of gold and the surface tension of the passivating gold layer are key parameters controlling this process. Adsorption phenomena exhibit strong influences on these variables, as is evidenced by changes in the critical potential. In comparison to sulfate and perchlorate media, chloride decreases the critical potential while derivatization of Cu_3Au with an alkyl-thiol increases it. These shifts are consistent with the enhancement and inhibition of the surface mobility of gold by the respective adsorbates. This description provides a rational basis for corrosion inhibition,

i.e., control of surface mobility by adsorption. For a given system, this may be further extended by minor alloying with elements which have beneficial adsorption/diffusion characteristics.

REFERENCES

1. H. Kaiser, in "Corrosion Mechanisms," F. Mansfeld, Editor, Marcel Dekker, Inc., New York (1987).
2. H. W. Pickering, *Corros. Sci.*, **23**, 1107 (1983).
3. (a) T. B. Cassagne, W. F. Flanagan, and B. D. Lichter, in "Chemistry and Physics of Fracture," R. M. Latanision and R. H. Jones, Editors, p. 659, Martinus Nijhoff Publishers, Boston (1987); (b) R. C. Newman and K. Sieradzki, *ibid.*, p. 597.
4. (a) A. D. Tomsett, D. J. Young, and M. S. Wainwright, *This Journal*, **131**, 2476 (1984); (b) J. Szot, D. J. Young, A. Bourdillon, and K. E. Easterling, *Philos. Mag. Lett.*, **55**, 109 (1987).
5. H. W. Pickering and C. Wagner, *This Journal*, **114**, 698 (1967).
6. C. Wagner, *ibid.*, **101**, 225 (1954).
7. (a) R. P. Tischer and H. Gerischer, *Z. Elektrochem.*, **62**, 50 (1962); (b) H. Gerischer and H. Rickert, *Z. Metallkunde*, **46**, 681 (1955).
8. A. J. Forty and P. Durkin, *Philos. Mag. A*, **42**, 295 (1980).
9. A. J. Forty and G. Rowlands, *ibid.*, **43**, 171 (1981).
10. (a) M. J. Pryor and J. C. Fister, *This Journal*, **131**, 1230 (1984); (b) D. J. Keir and M. J. Pryor, *ibid.*, **127**, 2138 (1980).
11. K. Sieradzki, R. R. Corderman, K. Shukla, and R. C. Newman, *Philos. Mag. A*, **59**, 713 (1989).
12. B. Kabius, H. Kaiser, and H. Kaesche, in "Surfaces, Inhibition and Passivation," E. McCafferty and R. J. Brodd, Editors, PV 86-7, p. 562, The Electrochemical Society Softbound Proceedings Series, Pennington, NJ (1986).
13. H. Gladen, H. Kaiser, and H. Kaesche, *Corros. Sci.*, **30**, 737 (1990).
14. T. R. I. Cataldi, I. G. Blackham, G. A. D. Briggs, J. B. Pethica, and H. A. O. Hill, *J. Electroanal. Chem.*, **290**, 1 (1990).
15. H. W. Pickering and P. J. Byrne, *This Journal*, **118**, 209 (1971).
16. B. W. Parks, J. D. Fritz, and H. W. Pickering, *Scripta Metall.*, **23**, 951 (1989).
17. (a) K. Hashimoto, *Corros. Sci.*, **5**, 597 (1965); (b) K. Hashimoto, T. Goto, W. Suetaka, and S. Shimodaira, *Trans. Jpn. Inst. Metals*, **6**, 107 (1965).
18. B. D. Cullity, "Elements of X-Ray Diffraction," 2nd ed., Addison-Wesley Pub., Reading, MA (1978).
19. F.-R. F. Fan and A. J. Bard, *This Journal*, **136**, 3216 (1989).
20. A. J. Bard and F.-R. F. Fan, in "Scanning Tunneling Microscopy," D. Bonnell, Editor, VCH Publishers, New York, In press.
21. A. A. Gewirth, D. H. Craston, and A. J. Bard, *J. Electroanal. Chem.*, **261**, 477 (1989).
22. (a) W. H. Smyrl, in "Comprehensive Treatise of Electrochemistry," Vol. 4, J. O'M. Bockris, B. E. Conway, E. Yeager, and R. E. White, Editors, p. 97, Plenum Press, New York (1981); (b) U. Bertocci and D. R. Turner, in "Encyclopedia of Electrochemistry of the Elements," Vol. VII, A. J. Bard, Editor, Marcel Dekker, Inc., New York (1974).
23. A. De Agostini, E. Schmidt, and W. J. Lorenz, *Electrochim. Acta*, **34**, 1243 (1989).
24. (a) D. M. Kolb, M. Przasnyski, and H. Gerischer, *J. Electroanal. Chem. Interfacial. Electrochem.*, **54**, 25 (1974); (b) D. M. Kolb, in "Advances in Electrochemistry and Electrochemical Engineering," Vol. 11, H. Gerischer and C. W. Tobias, Editors, p. 125, Wiley, New York (1978).
25. J. Laurent and D. Landolt, *Materials Science Forum*,

44/45, 213 (1989).

26. J. Laurent and D. Landolt, *Electrochim. Acta,* **36,** 49 (1991).
27. R. Bakish and W. D. Robertson, *J. Metals,* 1277 (1956).
28. R. J. Nichols, O. M. Magnussen, J. Hotlos, T. Twomey, R. J. Behm, and D. M. Kolb, *J. Electroanal. Chem.,* **290,** 21 (1990).
29. J. Wiechers, T. Towney, D. M. Kolb, and R. J. Behm, *ibid.,* **248,** 451 (1988).
30. D. J. Trevor, C. E. D. Chidsey, and D. N. Loiacono, *Phys. Rev. Lett.,* **62,** 929 (1989).
31. H. Honbo, S. Sugawara, and K. Itaya, *Anal. Chem.,* **62,** 2424 (1990).
32. I. Otsuka and T. Iwasaki, *J. Vac. Sci. Technol.,* **A8,** 530 (1990).
33. M. D. Porter, T. B. Bright, D. L. Allara, and C. E. D. Chidsey, *J. Am. Chem. Soc.,* **109,** 3559 (1987).
34. C. Alonso, R. C. Salvarezza, J. M. Vara, and A. J. Arvia, *Electrochim. Acta,* **35,** 1331 (1990).
35. S. Stucki, *J. Electroanal. Chem. Interfacial. Electrochem.,* **78,** 31 (1977).

36. R. W. Balluffi and J. W. Cahn, *Acta Metall.,* **29,** 493 (1981).
37. N. Sato, *This Journal,* **129,** 255 (1982).
38. J. R. Galvele, *Corros. Sci.,* **27,** 1 (1987).
39. H. W. Pickering, *This Journal,* **7,** 690 (1968).
40. A. D. Tomsett, D. J. Young, M. R. Stammbach, and M. S. Wainwright, *J. Mater. Sci.,* **25,** 4106 (1990).
41. H. W. Pickering and P. R. Swann, *Corrosion,* **19,** 373t (1963).
42. B. D. Lichter, W. F. Flanagan, J. B. Lee, and M. Zhu, in "Environment-Induced Cracking of Metals," NACE-10, R. P. Gangloff and M. B. Ives, Editors, NACE, Houston, TX (1990).
43. R. G. Kelly, A. J. Young, and R. C. Newman, Abstract 213, p. 310, The Electrochemical Society Extended Abstracts, Vol. 90-2, Seattle, WA, Meeting, Oct. 14-19, 1990, and *This Journal,* **137,** 382C (1990).
44. J. D. Fritz, B. W. Parks, and H. W. Pickering, *Scripta Metall.,* **22,** 1063 (1988).
45. K. Sieradzki, J. S. Kim, A. T. Cole, and R. C. Newman, *This Journal,* **134,** 1635 (1987).

Anodic Polarization Behavior of Copper in Aqueous Chloride/Benzotriazole Solutions

Desmond Tromans* and Ru-hong Sun

Department of Metals and Materials Engineering, The University of British Columbia, Vancouver, British Columbia, V6T 1W5, Canada

ABSTRACT

Potential-pH equilibria and potentiodynamic polarization studies were used to confirm that formation of $CuCl_2^-$ complexes in $1.0M$ NaCl and $0.1M$ NaCl solutions produces a range of potentials at which anodic dissolution of copper occurs without formation of oxide. The interaction of benzotriazole (1 g/l) with oxide-free copper surfaces in the chloride solutions was studied by potentiodynamic polarization and potentiostatic techniques. Inhibition of the anodic dissolution reaction was obtained in near-neutral pH solutions and at pH 3.0. Inhibition was ineffective at pH 1.0. The interaction of benzotriazole with oxide-free surfaces, leading to inhibition, was potential- and time-dependent. Also, a limiting potential was observed and predicted above which additions of benzotriazole are ineffective and above which existing inhibiting films cannot undergo spontaneous repair. The results confirm that benzotriazole can interact with oxide-free surfaces to promote corrosion inhibition of copper. The characteristics of the inhibition behavior, including breakdown and pH effects, were consistent with an inhibiting film that formed by adsorption of neutral benzotriazole molecules onto the Cu surface, followed by the adsorption of a thin layer of cuprous benzotriazole in polymeric form.

Chloride ions are known to promote the aqueous corrosion of copper (1-3), whereas benzotriazole $C_6H_4N_3H$) is one of the most widely used agents for inhibiting such corrosion (4, 5). Commencing with the pioneering work of Cotton and co-workers (6, 7), many investigations relating to the inhibition phenomenon have been published. These include comparative electrochemical and corrosion studies in the presence and absence of benzotriazole (4, 8-15), the adsorption behavior of benzotriazole (11, 15, 16), ellipsometric studies of corrosion films (4, 17), and several composition and structural investigations of reaction films using the techniques of infrared spectroscopy (IRS) (9, 10, 18, 19), electron spectroscopy (ES) (10, 11, 20, 21), and Raman spectroscopy (15, 22-24). In addition, the interactions of copper oxide substrates with solutions containing benzotriazole have been studied by ES (11, 25). Also, the structures of adsorbed films produced by vacuum deposition of benzotriazole onto sputter-cleaned copper oxide and copper substrates have been studied by IRS (26, 27) and ES (27) techniques.

The early studies by Cotton *et al.* (6, 7) postulated that the corrosion-inhibiting effect of benzotriazole is due to the formation of thin (<5 nm) chemisorbed polymeric films of Cu-benzotriazole complexes. Poling (9) confirmed that the complexes contain cuprous species and that the films may reach thicknesses up to 500 nm. Mansfeld and Smith (17) showed that film thickness is pH-dependent, being thin in neutral chloride solutions and thicker at

lower pH. Work by Youda *et al.* (15, 24) in sulfate solutions indicated that complex polymer films are formed at higher potentials and pH values, whereas benzotriazole molecules are adsorbed at lower values.

Following suggestions that cuprous oxide (Cu_2O) surface films are necessary for the reaction of benzotriazole with copper (9, 17), Ogle and Poling (10) showed that cuprous-benzotriazole polymeric films could be grown on Cu_2O interfaces in chloride solutions and that the pH-dependent growth of the polymeric films on copper is linked to the stability of Cu_2O. Other workers (11, 19, 20, 25) have since shown that a Cu_2O interlayer facilitates the formation of polymeric films, whereas Hashemi and Hogarth (21) believe that a cuprous chloride (CuCl) interlayer is necessary. Confirmation of the chemisorption of benzotriazole on clean Cu_2O substrates in the absence of an aqueous environment has been obtained by Fang *et al.* (26) and Nilsson *et al.* (27). However, these workers (26, 27) also showed that under the same conditions chemisorption occurred on clean copper substrates.

The degree to which benzotriazole will interact with oxide-free copper surfaces in an aqueous environment and inhibit electrochemical processes is unclear from the published literature. Furthermore, it is equally uncertain whether such an interaction is rapid and/or potential-dependent. In principle, cathodic reduction could be used to remove the initial air-formed oxide film. However, it must be done before the addition of inhibitor to the solution, because interaction of benzotriazole with Cu_2O is reported to be rapid (20). In the majority of situations where

* Electrochemical Society Active Member.